中國機械工程學刊第三十九卷第三期第 267~274 頁(民國一百零七年)
Journal of the Chinese Society of Mechanical Engineers, Vol.39, No.3, pp 267~274 (2018)

Fabrication and Evaluation of Reflected Type Optical Linear Encoder Using Femtosecond Laser

Mohammad Hossein Goudarzi *, Jeng-Ywan Jeng** and Ji-Bin Horng***

Keywords： Femtosecond phenomena, Diffraction gratings, Talbot and self-imaging effects.

ABSTRACT

This paper explains the fabrication method of linear diffraction grating by femtosecond laser. Several gratings were made using two setups: chirped pulse FS laser and mode locked fibre laser. Laser direct writing with different optical paths was used to fabricate two gratings with pitches of 5mm and 20mm. The average power, scanning speed and repetition rate of the laser were changed to determine optimal grating. The ablation threshold of Invar36 was calculated for NOPs of 389 and 1.1, resulting in 0.122J/cm^2 and 0.42 J/cm^2 respectively. And an online non-destructive performance testing procedure was applied to assess the reflective diffraction grating for optical linear encoding applications, based on the Talbot effect. The contrast of self-imaging was used as a comparison parameter. These results were verified by measuring the diffraction efficiency and traveling distance, using a Renishaw encoder. The best and poorest samples were the same in all setups, as was the trend. Specifically, the worst case couldn't deliver a self-image with acceptable contrast, or generate uniform signals from an optical Tonic read head, since it diffracted laser light to different points and its diffraction efficiency was very low. In addition, the traveling distance error of the best sample was only 0.1mm.

Paper Received June, 2017. Revised Sepfember, 2017. Accepted October, 2017. Author for Correspondence: Mohammad Hossein Goudarzi

* *PhD student, Department of Mechanical Engineering, National Taiwan University of Science and Technology, Taipei, Taiwan, ROC.*

***Professor, Department of Mechanical Engineering, Engineering School, National Taiwan University of Science and Technology, Taipei, Taiwan, ROC.*

****Doctor, Industrial Technology Research Institute (ITRI) , ITRI Southern Region Campus, 8 Gongyan Road, Liu-jia District, Tainan, Taiwan 73445ROC.*

INTRODUCTION

Many current optical encoders are based on the Talbot effect and self-imaging properties, which are the largest markets for 1D diffraction grating (Crespo et al, 2000; Sanchez-Brea et al, 2009; Heidenhain Co. 2015; Ye et al, 2015; Kao et al, 2010; Kao et al, 2005). According to the Talbot effect, the image of periodic microstructures such as gratings appears at the Talbot distance in the Fresnel diffraction Region (Liu et al, 1989). Many theoretical and experimental studies have discussed the influence of grating size and phase modulation on the Talbot effect, as well as how to observe the effect. Using a 10 tip fibre probe mounted in PZT and a CCD/CMOS camera is a popular technique for observing the Talbot effect (Luo et al, 2005; Guerineau et al, 2000, Wei et al, 2009; Wei et al, 2006). Some researchers used Talbot interferometry to measure the tilt and roll angle of two gratings, or their parallelism (Liu et al, 1999; Liu et al, 2007). Defects such as missed or dislocated fringes with Talbot effect were also studied (Teng et al, 2014). The fringes were considered stationary, and they studied the defects according to application of reflecting diffraction grating in a linear optical encoder. The definition of defects and tolerance of missed or un-located fringes can be different with fixed grating. In order to determine an online, low-cost and non-destructive performance testing method, this paper considers the self-imaging properties of grating under IR LED illumination with viewing angle of 60°, which allows observation of detects on each pitch independently.

Over the past decade, high precision (1 nm resolution) optical encoders have employed a 36% Ni-Fe alloy (Invar 36) scales in off-plane diffraction grating configurations. The thermal expansion coefficient (CTE) of Invar is very low at ambient temperature (CTE_{RT} =1.8×10^{-6}/°C), and this thermal stability has encouraged its use in precision industries to minimize temperature related errors (Lu et al, 2007; Renishaw website). Thus, the effect of temperature is not significant on this substrate. In the range of a nanosecond pulsed laser, the heat affected zone in metal is very large, the molten material creates debris and the line edges are not precise enough for optical components (Nolte et al, 1997; Lee et al, 2009). Since the heat affected zone is negligible with the ultrashort pulsed laser, and there is no debris from molten material, it can make precise and high quality lines since it's cold machining process is due to the extreme electrical field of the femtosecond pulse and the very short pulse width (Seea et al, 2015; Eaton et al, 2015; Li et al, 2010). The pulse width of less than 120 fs and energy greater than 10^{13}-10^{14} W.cm^{-2} is suitable for cold machining (Gamaly et al, 2009). In this study, two different laser sources with pulse widths of 500 fs and 120 fs were used to fabricate gratings on Invar for the optical encoder scale.

This study explains the fabrication method of gratings for encoder application by FS laser in detail, and the calculated ablation threshold of Invar for high performance grating according to critical FS laser parameters. It also describes a special method to measure fabricated gratings with the Talbot effect. This measuring method involves a performance testing setup for evaluating the suitability and adaptability of linear diffraction gratings for linear encoder applications. Some features, such as fringe depth, are not defects but still affect the performance of gratings, and some defects, including dots and particles, have minimal effect on the performance of gratings in the optical encoder application. The results of this method were compared by measuring the intensity and position of diffracted points in an off-plane diffraction configuration. A commercial optical read head was used to compare distance and traveling distance.

EXPERIMENTAL SETUP

Fabrication Setup, The sample preparation is done by a JY150MP polishing machine and two different FS laser sources and their different optical paths and other accessories were used to make micro-structure pattern and an ultrasonic alcohol bath were used for post cleaning process. The JY150MP polished the surface of 1.1 mm thick single Invar 36 substrate, to create a mirror surface with surface roughness under 15 nm. Fifteen diffraction gratings with 20 µm pitch were then fabricated by the mode locked fibre FS laser (Fianium HE1060-2µJ-fs). A 10× objective lens (Mitutoyo NA 0.14, MPLAN APO NIR) focused laser beam from 5.5mm to 8.5µm spot size on the Invar sample, which was located on an X-Y motorized stage with accuracy of 0.5 µm. The repetition rate f was set from 1 MHz×1/n for n = 1, 2 . . . 9, and the range of pulse energies was from 0.23 µJ to 1.59 µJ when the pulse duration was fixed at 350 fs. The scan speed ϑ also varied, from 1 mm/s to 22 mm/s.

Three different diffraction gratings with 2.5mm line width were fabricated by a chirped-pulse amplified Ti:sapphire FS laser. The pulse duration was fixed at 120 fs, and the central wavelength was 800nm at a pulse repetition rate of 1000Hz. FS lasers with pulse periods less than 200 fs provide a high precision cold machining method that requires very low laser fluence to start the ablation process, and results in sharply machined edges that increase the efficiency of the diffraction gratings (Li et al, 2010; Gamaly et al, 2009).

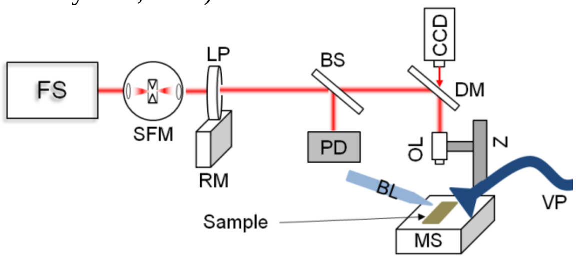

Fig. 1. Fabrication setup for making 5um pitch on the Invar; FS: femtosecond laser, SFM: Spatial filtering mechanism, LP: Linear Polarizer, RM: Rotary motorized stage, BS: Beam splitter 4%, PD: Power detector, DM: Dichroic mirror, OL: Objective lens 50x

A pinhole aperture with diameter of 200µm was used for spatial beam filtering before adjusting the power. The pinhole and two related lenses were located inside a vacuum chamber, and provided a beam profile of passed light that was close to an ideal Gaussian beam profile. The light power of the laser was adjusted using a linear polarizer mounted on a precise motorized rotary stage. The maximum pulse energy was 3mJ, and the polarization direction was along the grating lines. A 50x objective lens (Mitutoyo NA 0.42, PLAN APO SL) was employed at the end of the optical path, and its spot size was approximately 2.2µm due to refraction of the 800nm wavelength. Both laser direct writing setups used a nitrogen gas blower and a vacuum pipe as a debris-control system to collect ions, plasma plumes and evaporated particles (Fig. 1).

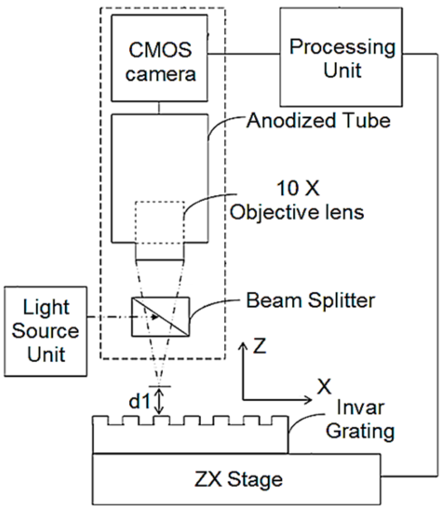

Fig. 2. Observation setup of capturing online and continuously

Observation Setups, Figure 2 shows the first experimental setup. The circular polarized IR LED (wave length of 850 nm, viewing angle of 60°) light is reflected by a beam splitter and irradiated on the fabricated reflecting gratings, with normal incidence with respect to the surface of grating. The diffracted light passes through the beam splitter and is captured by a CMOS camera (UI-1240LE-NIR-GL, pixel size 5.3×5.3 μm, 50% sensitivity at 850 nm) with an objective lens (Nikon Japan LU Plan Flour 10×/0.3). To increase the magnification to 30×, a tube of specific length was located between the camera and the objective lens, and diffracted light noise was removed by anodizing the inside of the tube to black. The gratings were located on an XY motorized stage with accuracy of 1 μm and resolution of 0.05 μm.

The second observation setup measured the diffraction efficiency of samples in off-plane diffraction configurations. The light source was a red DPSS laser (671nm by 65mW), and the incident laser beam diffracts from the off-plane grating to form coherent spots on the surface of the sphere (Rothenbach et al, 2015). Samples were placed at the centre of the sphere, and the light sensor power meter was installed on the tilt mount perpendicular to the diffracted beam. The tilt mount was moved by the linear X-Y motorized stage to different positions of the diffracted beam. The plane of the motorized stage is perpendicular to the surface of the grating, but at an appropriate distance away. Thus, the optical paths of all diffracted beams are the same in this setup.

The third setup was used to compare the traveling distance between the fabricated grating and a commercial high precision motorized stage with a glass scale. The setup included a linear motorized stage (Thorlab-DDS600 with glass scale) and a Renishaw Tonic read head (TONIC T1011-15A), and compared the traveling distance of two different optical linear encoders (i.e. the DDS600 stage, and the TONIC read head). The Tonic read head interpreted the gratings on the Invar, and the results were compared with the DSS600 results. The traveling distance for each sample was from 1 to 2 mm (Fig. 3.).

While the different laser parameters altered the surface roughness of the laser affected zone, the surface roughness of the reflecting area of gratings, the non-laser affected zone, was unchanged. Therefore, this study did not consider the effect of surface roughness. Finally, the substrate was cleaned in an alcohol ultrasonic bath at 32°C.

Discussion

Laser ablation threshold, The ablation threshold was calculated according to the line width of the laser affected zone. Figure 4a shows the line width and depth of a grating of 5um pitch and 2.5um line width by a confocal Olympus laser OM with 100X magnification, and Figures 4b, c and d show the line width of gratings of 20um pitch by a confocal Keyence laser OM with 50X magnification. Two different morphologies are observed by increasing the laser fluence, and the high energy regime occurs at the centre of the beam, due to the nature of Guassian beams. This high energy regime can remove material easily, while the low energy regime can change the colour of the surface, which decreases the grating efficiency.

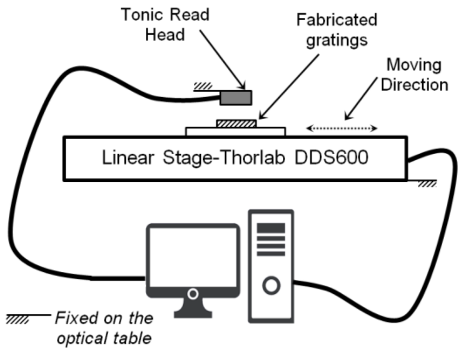

Fig. 3. measuring setup for comparing optical glass scale of Thorlab DDS600 by fabricated grating with Renishaw Tonic Read head**.**

The line width is related to the peak laser fluence, and increasing the laser fluence increases the line width according to a logarithmic trend $D^2 = 2\omega_0^2 \ln\left(\frac{H_0}{H_{th}}\right)$. The pulse energy also is related to peak laser fluence as follows:

$$H_0 = \left(\frac{2E_p}{\pi\omega_0^2}\right)$$

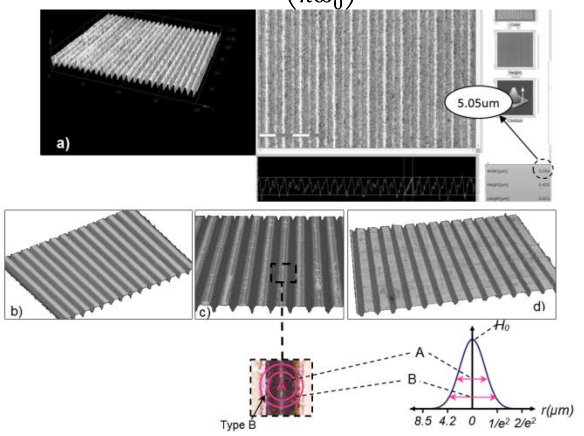

Fig. 4. Fringes of different grating under a confocal OM laser with different pitches:
a) H0=0.41 J/cm², NOP= 11, Depth= 0.43μm, Width=2.5μm
b) H0=0.2 J/cm², NOP= 389, Depth= 2μm, Width=10μm,
c) H0=0.57 J/cm², NOP= 194, Depth= 4.98μm, Width=11.5μm,
d) H0=0.2 J/cm², NOP= 71, Depth= 0.69μm, Width=11.47μm,
e) Two types of morphology, the material has been removed in A region and the discoloration has been happened in B region.

Since the line width is related to the pulse energy ($D^2 = 2\omega_0^2 \ln\left(\frac{E_p}{E_{th}}\right)$), and the beam spatial radius (ω_0) is related to the number of pulses (NOP).The ω_0 can be obtained by drawing D^2 against the logarithm of pulse energy with a constant NOP. This was 7.2 µm for an NOP of 389, and 3.41µm with an NOP of 1.1. The NOP of 389 was fabricated with a mode locked fibre laser at a wavelength of 1064nm and an objective lens magnification of 10X, and the NOP of 1.1 was fabricated with a chirped pulsed laser at a wavelength of 800nm with a 50X objective lens.

The laser ablation threshold can be obtained by plotting D^2 against the logarithm of peak laser influence. The intersection of the fitted line to this curve and the horizontal axis is the laser ablation threshold. This calculation method was detailed in our previous article.

As shown in Figure 5, the ablation threshold of 0.122 J/cm^2 was obtained for an NOP of 389 at a repetition rate of 1MHz and scan speed of 22mm/s, and the laser ablation threshold of 0.42 J/cm^2 was obtained for an NOP of 1.1 at a repetition rate of 1 KHz and scan speed of 2mm/s. The type of laser and optical paths were different in the two experiments: one was a mode locked fibre laser and the other was a chirped pulse laser with different optical paths and lens magnifications. Results showed that the laser ablation threshold of Invar has good agreement with previous studies on the nickel alloys, and that the ablation threshold is not related to the type of FS laser.

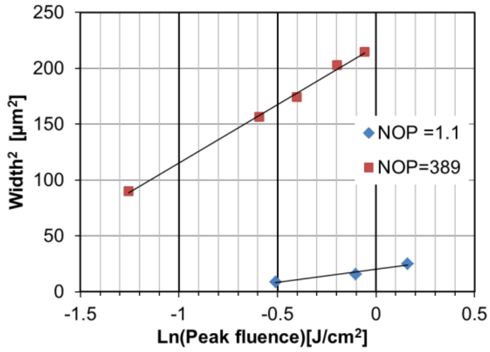

Fig. 5. The ablation threshold of NOP of 1.1 and NOP of 389.

Performance Testing Method, As seen in Figure 2, the camera focused on the grating when the grating fringes were set parallel to the camera pixels, by rotating the grating around its yaw axis. We used a CMOS camera in live mode to check the perpendicularity of the gratings to the light path by moving the grating along the X axis for an extended distance (15cm), and checking the sharpness of the fringe edges. After alimenting, the optic axis is perpendicular to the plane of the gratings, and the fringes are parallel to the camera pixels. The camera captured 20 images per second, and the motorized stage moved 0.02 mm/s on the Z axis (Figure 2), so one image was captured for each mm distance. The Matlab software analysed the images using a specific algorithm.

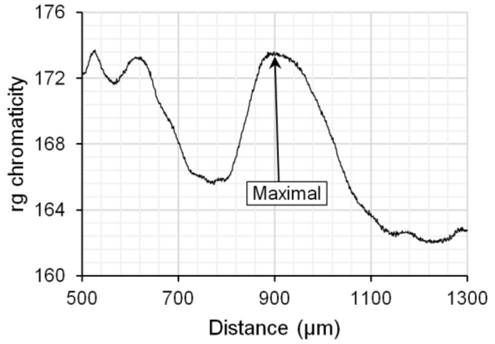

Fig. 6. Contrast curve along the Z axis smoothed by a special algorithm.

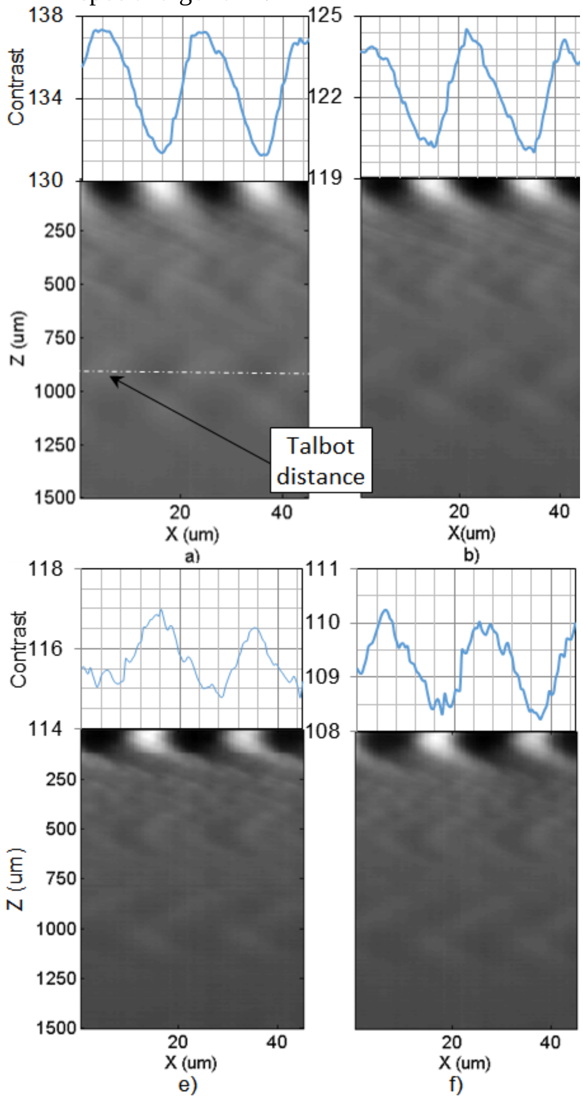

Fig. 7. X-Z slices of measured 3D intensity distributions: a to d is the same average power, and 1, 0.5, 0.11 and 0.1 MHz repetition rate, respectively.

The Talbot distance is the first distance where a self-image of a grating will appear in the same phase (Case et al, 2009) when the grating is illuminated by a plane wave. It is calculated as $Z_t = {2d^2}/{\lambda}$, where d is the pitch of the grating and l is the incident wavelength of the monochromatic light source. The central wavelength of the IR LED was 850 nm and the Talbot distance of the above formulation is 940µm. The image processing algorithm used this value to find exact position of first self-image which is where the chromaticity is maximum, as shown in Figure 6. The rg chromaticity was applied to the image in the Z direction to create a contrast curve, and a self-imaging distance of 900µm was defined at the maximum distance of the curve. The self-imaging distance was maintained at 900±35µm for all samples.

Figures 7 and 8 show X-Z slices of the measured 3D intensity distributions of the gratings. There is periodic intensity in the level of the self-imaging distances. The effect of the FS laser repetition rate and average power on the Talbot effect is also shown in Figures 7 and 8 respectively. As seen in Figure 7, decreasing the repetition rate decreases the uniformity of intensity curve, and the difference between the highest and lowest intensity is determined by comparing Figure 7a and Figure 7d. This trend is repeated with increasing average power (Figures 8a to 8b), which decreases both the uniformity of the intensity curve and the difference between the highest and lowest intensity.

This difference between the highest and lowest intensity is considered the ‘contrast’ in this article. Since different laser parameters were applied to produce each sample, the depth and width of the fringes of the samples were not equal. The different parameters and fringe features affect the contrast and diffraction grating efficiency.

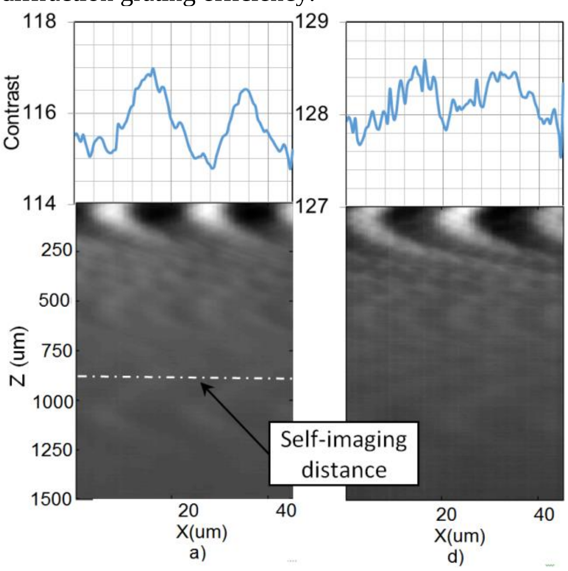

Fig. 8. X-Z slices of measured 3D intensity distributions for different laser parameters: a and d is the same repetition rate of 1 MHz, and 455, 775 mW/cm^2 average power, respectively.

As shown in Figure 9a, increasing the laser peak fluence of the FS laser decreases the contrast of the self-image at the first self-image distance in different regimes. Since we can set the average laser power, it is different for each sample. The average power was minimum (i.e. lowest laser peak fluence) for the best sample with respect to the contrast of the self-image, and it also had the lowest average power, the highest repetition rate and the highest scan speed. In our case this was the first sample, which had an average power of 230 mW/cm^2, a repetition rate of 1 MHz and a scan speed of 22mm/s, with a fringe depth of 4.12µm and a duty cycle of 52%.

The contrast of the self-image was not a function of the depth, it was decreasing the duty cycle that decreased the contrast (Figure 9c). As shown in Figures 7 and 8, the intensity of light was changed periodically in the level of the self-imaging distance. A sine function was fitted to the intensity of the distance level, and the R-squared value of this curve was used as a second comparison parameter. Figure 9b shows the effect of laser peak fluence on the R-squared value of the curve fitted function. This trend was also found in the sample produced with minimum laser peak fluence, which had an R-squared value of R^2 = 0.942. The diffraction grating efficiency for all samples in terms of laser peak fluence is shown in Figure 10.

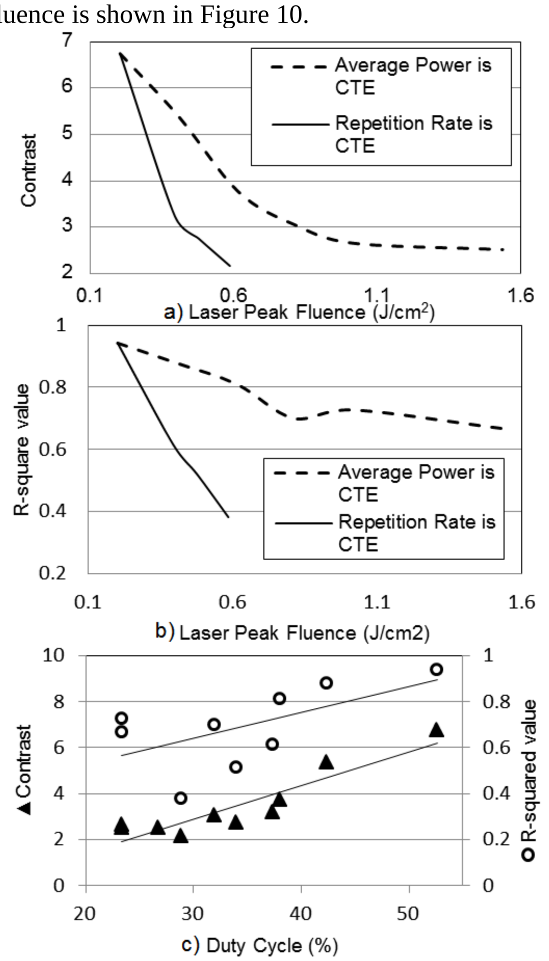

Fig. 9 The effect of laser peak influence on a) the

contrast of the self-image, b) the R-squared value of the self-imaging distance and c) the contrast and R-squared value according to the grating duty cycle.

The diffraction efficiency of the first sample (1MHz, 230mW/cm^2, 22mm/s) was maximum, and it was also the best sample with respect to contrast. As shown in Figures 9a and 10, the trend of the contrast and efficiency curves in this sample were the same, and these trends were also the same in the worst (10th) sample, though it didn't fit to a sine curve (R^2=0.02). Thus, the contrast of the self-image at self-imaging distance can be a powerful parameter to evaluate the grating in encoder and scale applications.

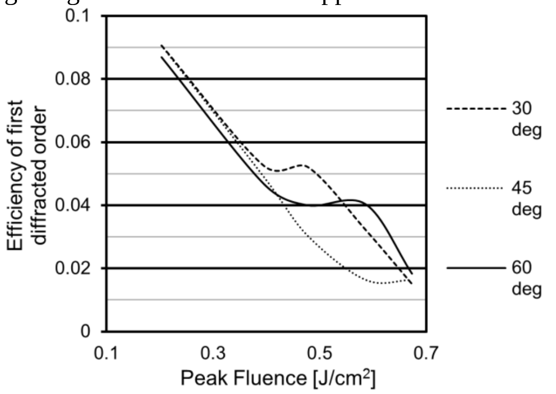

Fig. 10. Effect of laser influence on the diffraction efficiency of gratings

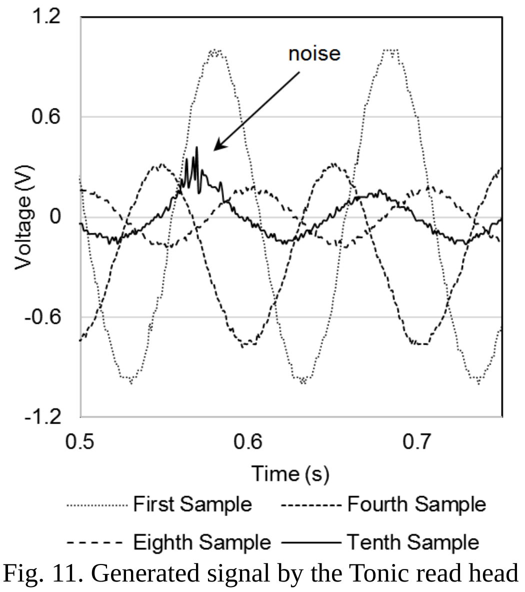

Fig. 11. Generated signal by the Tonic read head

Table 1. Displacement error differences in the reported positions of the DDS600 stage and the Tonic read head

Displacement Error					
Sample No.	Traveling distance	Error	Sample No.	Traveling distance	Error
1	1.91	100	9	1.68	1520
2	1.80	200	10	1.73	NAN
3	1.92	220	11	1.92	550
4	1.85	280	12	1.87	830
5	1.43	870	13	1.93	880
6	1.76	820	14	1.83	850
7	1.82	2110	15	1.78	790
8	1.63	1530			

These gratings were also compared with another optical encoder on the Thorlab DDS600 stage (Figure 3). The generated signal of the first channel, shown in Figure 11a, was very strong and uniform. It had an error rate of 0.1 mm in a traveling distance of 1.91mm, as seen in the Table 1. The diffraction efficiency of the worst sample (1MHz, 755 mW/cm^2, 22mm/s) was 0.02. This sample did not generate a uniform signal due to excessive noise, and was unable to report the traveling distance of the Tonic read head. This noise has been repeated periodically.

CONCLUSIONS

Two series of gratings were fabricated with pitch of 5μm and 20μm by chirped pulsed fs laser and mode locked fibre FS laser respectively. The laser ablation threshold of Invar was calculated for two different laser setups and the amount and trend of laser ablation threshold were in good agreement by previous studies for nickel alloys. It was shown that the laser ablation threshold of Invar was 0.42 J/cm^2 for NOP of 1.1 and scan speed of 2mm/s when the repetition rate was 1KHz and it was 0.122 J/cm^2 for NOP of 389 and scan speed of 22mm/s. Fifteen linear gratings (scale) were fabricated by different FS laser parameters with pitch of 20μm, and were evaluated by:

- the contrast of the self-image in Talbot distance;
- the R-squared of the sine curve fitted;
- the efficiency of off-plane diffraction configurations; and,
- comparisons with two different optical encoders.

Though the best and worst cases in all methods were the same, the seventh sample had the best diffraction efficiency (2nd place) with maximum traveling error, and was 5th in terms of the contrast of the self-image and R-squared value. Thus, the contrast of the self-image is an acceptable procedure to evaluate scale and efficiency. The 10th sample (worst case) diffracted incident laser light to points and had very low diffraction efficiency (0.02), but it was not a suitable encoder scale because it was unable to generate a uniform and stable signal. So the threshold value of contrast for this optical setup is 0.8. The self-imaging setup can determine the location of defects to a resolution of 10 pitches. This means that the focused area of this setup is approximately 10 pitches, and it can observe effective defects smaller than 2mm of scale with an optical encoder application on each pitch. The results show that this method of analyzing self-image contrast is inexpensive, simple and fast. Thus, it could be used as an online QC tool for a scale manufacturing company.

REFERENCES

Crespo, D., Alonso, J., Morlanes, T., and Bernabeu, E., “Optical encoder based on the Lau effect,” Optical Engineering, Vol. 39, pp. 817–824, 2000.

Sanchez-Brea, L. M. Torcal-Milla,, F. J., and Bernabeu, E., “Continuous self-imaging regime with a doublegrating mask,” Applied Optics, Vol. 48, No. 30, pp. 5722-5727, 2009. doi:10.1364/AO.48.005722

Heidenhain Co. 2015. Exposed Linear Encoders catalogue of Heidenhain. Accessed September 2. http://www.heidenhain.com/en_US/products-and-applications/linear-encoders/exposed-linear-encoders/

Ye, G. Y., Liu, H. Z., Fan, S. J., Li, X., Yu, H. Y., Lei, B., Shi, Y. S., Yin, and Lu,B. H. , “A theoretical investigation of generalized grating imaging and its application to optical encoders,” Optics Communications, Vol. 354, pp. 21–27, 2015.

Kao, C. F., and Lu, S. H., “Reflective-type optical encoder based on fractional Talbot selfimage effect using phase grating,” In Proceeding of SPIE, Vol. 7544 No. 75440N, 2010. doi: 10.1117/12.886238.

Kao, C. F., and Lu, M. H., “Optical encoder based on the fractional Talbot effect,” Optics Communications, Vol. 250, pp. 16-23, 2005.

Liu, L., “Talbot and Lau effects on incident beams of arbitrary wavefront and their use,” Applied Optics, Vol. 28, pp. 4668–4678, 1989. doi:10.1364/AO.29.004337.

Luo, H. X., Zhou, C. H., Zou, H., and Lu, Y. Q, “Talbot-SNOM method for non-contact evaluation of high-density gratings,” Optics Communications, Vol. 248, pp. 97–103, 2005. doi:10.1016/j.optcom.2004.12.004.

Dubey, S. K., Mehta, D. S., Roy, A., and Shakher, C., “Wavelength-scanning Talbot effect and its application for arbitrary three-dimensional step-height measurement,” Optics Communications, Vol. 279, pp. 13–19, 2007.

Guerineau, N., Harchaoui, B., and Primot, J., “Talbot experiment re-examined: demonstration of an achromatic and continuous self-imaging regime,” Optics Communications, Vol. 180, pp. 199–203, 2000.

Wei, W. A., Zhou, C. H., Dai, E. W., and Bai, B., “Talbot effect under illumination of double femtosecond laser pulses,” Optik, Vol. 120, pp. 625–629, 2009. doi:10.1016/j.ijleo.2008.02.014.

Wei, W. A., Zhou,C. H., Dai, E. W., and Liu, W. J., “Experimental study of the Talbot effect under femtosecond laser illumination,” Optics Communications, Vol. 260, pp. 415–419, 2006. doi:10.1016/j.optcom.2005.11.021

Liu, Q. A., and Ohba, R. J., “The effect of arbitrary small discrepancy between normal directions of grating planes in Talbot interferometry,” Optics Communications, Vol. 170, pp. 193–199, 1999.

Liu, Q. A., and Ohba, R. J., “A simple real-time method for checking parallelism between the two gratings in Talbot interferometry,” Optics Communications, Vol. 175, pp. 19–26, 2007. doi:10.1016/S0030-4018(99)00757-9.

Teng, S. Y., Wang, J. H., Zhang, W., and Cui, Y. W., “Talbot effect of the defective grating in deep Fresnel region,” Optics Communications, Vol. 336, pp. 213–223, 2014. doi:10.1016/j.optcom.2014.10.013.

Lü, T., and Yang, S., “Extrinsic Fabry–Perot cavity optical fiber liquid-level sensor," Applied Optics, Vol. 46, No. 18, pp. 3682-3687, 2007. doi:10.1364/AO.46.003682

http://www.renishaw.com/en/tonic-relm-linear-encoder-system–10236.

Nolte, S., Momma, C., Jacobs, H.,Tünnermann, A., Chichkov, B. N., Wellegehausen, B., and Welling, H., “Ablation of metals by ultrashort laser pulses,” JOSA B. Vol. 14, No. 10, pp. 2716-2722, 1997. doi:10.1364/JOSAB.14.002716.

Lee, H., Jeong, Y. U., and Chan, K. F., “The Advent of Laser Therapies in Dermatology and Urology: Underlying Mechanisms, Recent Trends and Future Directions,” Journal of the Optical Society of Korea, Vol. 13, No. 3, pp. 321-329, 2009.

Seea, T.L., Liua, B. Z., Liua, H., Lib, L., Chippendalec, J., Cheethamc, S., Dilworthc, S., “Effect of geometry measurements on characteristics of femtosecond laser ablation of HR4 nickel alloy,” Optics and Lasers in Engineering, Vol. 64, pp. 71–78, 2015.

Eaton,S., Zhang, H., Herman, P., Yoshino, F., Shah, L., Bovatsek, J., and Arai, A., “Heat accumulation effects in femtosecond laser-written waveguides with variable repetition rate,” Optics Express, Vol. 13, No. 12, pp. 4708-4716, 2015.

Li, Z., Li, P., Fan, J., Fang, R., Zhang, D., “Energy accumulation effect and parameter optimization for fabricating of high-uniform and large-area period surface structures induced by femtosecond pulsed lase." Optics and Lasers in Engineering, Vol. 48, No. 1, pp. 64–68, 2010. doi:10.1016/j.optlaseng.2009.07.017

Gamaly,E., Rode,A., Luther-Davies, B., and Tikhonchuk, V., "Ablation of solids by femtosecond lasers: Ablation mechanism and ablation thresholds for metals and dielectrics," Phys. Plasmas. Vol.9, pp. 949, 2002. http://dx.doi.org/10.1063/1.1447555

Rothenbach, C., Kravchenko, I., Gupta, M., "Optical diffraction properties of multimicrogratings," Applied Optics, Vol. 54, No. 7, pp. 1808-1818, 2015. http://dx.doi.org/10.1364/AO.54.001808

Case, W. B., Tomand, M., Deachapunya, S., and Arndt, M., "Realization of optical carpets in the Talbot and Talbot-Lau configurations," Optics Express, Vol. 17, No. 23, pp. 20966-20974, 2009. doi:10.1364/OE.17.020966

NOMENCLATURE

d pitch of grating

D beam diameter, Width of fringes

f focal length of lens, repetition rate of pulsed laser

H_0 laser peak fluence

E_p Pulsed energy

H(r) laser fluence in the position of *r*

NOP number of pulse

r radial distance from beam center

λ wavelength

ω_0 laser spatial radius

ρ the spot size due to the diffraction

v scan speed

h the Planck constant

c the speed of light

θ_i angle of incident light to the grating

φ incident beam angles relative to the grating plane

α, β angle of diffracted order

飛秒雷射反射式光學線性編碼器的製作與評價

Goudarzi　鄭正元　洪基彬
臺灣科技大學機械工程學系

摘 要

本研究闡述了飛秒雷射器對線性衍射光柵的製作方法。使用兩種設置來製作幾個光柵：啁啾脈衝 FS 雷射器和鎖模光纖雷射器。使用不同光程的雷射，直接書寫在兩個間距分別為 5mm 和 20mm 的光柵上。調整雷射器的掃描速度和重複頻率，以平均功率確保光柵最佳化。對於 389 和 1.1 的 NOP，計算 Invar36 合金的燒蝕閾值，分別得到 0.122J/cm^{2}和 0.42J/cm^2。

基於泰伯(Talbot)效應，套用在線無損性能測試程序以評估光學線性編碼應用的反射式衍射光柵。使用自我成像的對比度為比較參數。通過使用 Renishaw 編碼器測量衍射效率和行進距離來驗證這些結果。所有設置中最好和最差的樣本都有相同的趨勢。具體而言，最壞的情況不能以可接受的對比度傳遞自身圖像，或者從光學 Tonic 讀數頭產生均勻的信號，因為它將雷射衍射到不同的點並且其衍射效率非常低。此外，最佳樣品的行程距離誤差僅為 0.1mm。